Manuscript Ref.: JELECHEM-D-20-00793

Electrosynthesis of hydrogen peroxide sustained by anodic oxygen evolution in a flow-through reactor

Oscar M. Cornejo [a], Ignasi Sirés [b], José L. Nava [a,*]

[a] *Departamento de Ingeniería Geomática e Hidráulica, Universidad de Guanajuato, Av. Juárez 77, Zona Centro, 36000, Guanajuato, Guanajuato, Mexico*

[b] *Laboratori d'Electroquímica dels Materials i del Medi Ambient, Departament de Química Física, Facultat de Química, Universitat de Barcelona, Martí i Franquès 1-11, 08028 Barcelona, Spain*

E-mail addresses: om.cornejorojas@ugto.mx (O.M. Cornejo)

i.sires@ub.edu (I. Sirés)

* Corresponding author's e-mail address: jlnm@ugto.mx (J.L. Nava)

Abstract

This study reports the performance of a flow-through reactor to promote the sustainable production of H_2O_2 upon cathodic reduction of anodically generated O_2. A smart configuration that alternated Ti|IrO_2-Ta_2O_5 anode meshes, as a source of O_2 subsequently reduced to H_2O_2 at adjacent porous reticulated vitreous carbon cathodes, was successfully tested employing a 0.050 M Na_2SO_4 solution at pH 3.0. With this reactor, the need of an external source of pure O_2 or air typically employed during the electrosynthesis of this high value commodity was avoided. Bulk electrolyses in recirculation operation mode were carried out to evaluate the influence of the volumetric flow rate (0.4-1.0 L min^{-1}) and applied current (59.5-178.5 mA) on the H_2O_2 accumulation profiles. The best performance of the reactor was achieved at 0.8 L min^{-1} and 59.5 mA, reaching 14.3 mg L^{-1} H_2O_2 after 3 h, with maximum current efficiency and electrolytic energy consumption of 100% and 0.021 kWh (g H_2O_2)$^{-1}$, respectively. This is a first approach to produce greener H_2O_2, envisaging its future application to water treatment by electrochemical advanced oxidation processes.

Keywords: Oxygen evolution reaction; Oxygen reduction reaction; Flow-through reactor; H_2O_2 electrogeneration; Water treatment

1. Introduction

Hydrogen peroxide is a very important chemical in our daily life due to its multiple industrial applications, such as mild synthesis of organic compounds, bleaching in paper and textile production, water disinfection and wastewater treatment [1,2]. As a green oxidant [3], H_2O_2 is an alternative to common toxic reagents like chromate or permanganate. In addition, several H_2O_2-based electrochemical oxidation processes like electro-Fenton (EF), photoelectro-Fenton and electro-peroxone have been successfully devised to produce hydroxyl radicals able to degrade organic pollutants in water [4-6] or create polymer gels [7].

In recent years, several plants have been built to produce H_2O_2 in order to satisfy the big demand from propene oxide synthesis [8], opening a huge market to new synthesis methods, although the most utilized at industrial scale is still the anthraquinone (AQ) autoxidation first described by Riedl and Pfleiderer in 1940 [9]. However, this method has some disadvantages, such as the use of solvents or the accumulation of unwanted harmful by-products [1]. Within this context, the electrosynthesis route has arisen as an eco-friendly alternative to chemical synthesis [2,10], being especially interesting when low to moderate H_2O_2 concentrations are required, as is the case of water treatment [11]. This typically involves the two-electron oxygen reduction reaction (ORR, (1)), which occurs with high efficiency at carbonaceous cathodes [12-17].

$$O_2 + 2H^+ + 2e^- \rightarrow H_2O_2 \qquad E^0 = 0.695 \text{ vs SHE} \qquad (1)$$

In many cases, these materials have been implemented in electrolytic cells in which the O_2 or air is fed into a gas chamber. The gas then flows from the back side of the porous cathode and is transformed into H_2O_2 at the three-phase boundary (i.e., in contact with the electrolyte). This configuration, so-called gas-diffusion electrodes (GDE), is known

to yield the greatest oxidant concentrations at ambient conditions [7,10,11,18-22]. Nonetheless, this technology is delicate due to possible cathode flooding if the pressures are not correctly balanced during the electrolysis [11], which typically obliges to employ expensive oversized compressors to fulfill the oxygen demand and air pressure. In such cases, this ends in an additional capital expense as well as a waste of energy from excessive air and liquid pumping [23]. However, it is worth mentioning that the proper design of the GDE in connection with a suitable compressor may decrease the cost of the external air supply.

In an electrochemical cell, the main event at the inert anode is the oxygen evolution reaction (OER, (2)). Dimensionally stable anodes (DSA) are the most widespread materials for this purpose [24].

$$2H_2O \rightarrow O_2 + 4H^+ + 4e^- \qquad E^0 = 1.229 \text{ V vs SHE} \qquad (2)$$

The O_2 evolution is commonly considered a side reaction with no added value. This is due to the electrode arrangement inside the reactor since they tend to be accommodated as parallel plates in flow-by reactors. Therefore, aiming to consume the O_2 produced at the anode to further favor the subsequent H_2O_2 electrosynthesis, a flow-through configuration with porous electrodes seems preferable. A first attempt was published by Drogui et al. [25], but a very simple cell equipped with a single graphite felt cathode was used. Recently, the concept has been demonstrated by Zhou et al. [26] employing a flow-through reactor equipped with a reticulated vitreous carbon (RVC) cathode. However, they observed some problems attributed to coalition of O_2 bubbles on the cathode surface, which was detrimental for the ORR as shown by their current efficiencies < 5%. In response to this limitation, this communication addresses the design of a smart rectangular flow-through cell to produce H_2O_2 in a more efficient manner. A novel flow-

through cell equipped with a porous Ti|IrO_2-Ta_2O_5 anode to form O_2 via OER, and an RVC cathode to yield H_2O_2 was evaluated in Na_2SO_4 medium at pH 3.0. The influence of the volumetric flow rate and applied current on the accumulation of H_2O_2, current efficiency and energy consumption was systematically assessed.

2. Materials and methods

Reagents of analytical grade were purchased from Sigma-Aldrich and Karal. Distilled water was used to prepare the analytical solutions and perform the electrolytic trials.

2.1. Description of the reactor

Fig. 1a shows an exploded view of the flow-through reactor, which was designed by ourselves based on computational fluid dynamics simulations. These are not shown herein, but they guaranteed good dispersion of the liquid, appropriate mass transport and homogeneous current distribution. Table 1 shows the dimensions and characteristics of the components of the reactor. The plastic elements were constructed by 3D printing, using acrylonitrile butadiene styrene (ABS).

The reactor was equipped with two pairs of anodes (A) and cathodes (C), arranged in an alternate A-C-A-C configuration (interelectrode gap of 0.5 cm) that ensured the adequate collection of the anodic O_2 at the cathode surface thanks to the vertical flow. The reactor consisted of two rectangular ABS end plates, whereas the electrolyte flow channel was embedded in between. As can be observed in Fig 1b, the electrolyte flow channel contained two sets of three Ti|IrO_2-Ta_2O_5 meshes, manufactured by the Pechini method [27], and two porous RVC pieces (Goodfellow, 60 pores per inch (ppi)). Both, anodes and cathodes had the same dimensions (1.5 cm length × 3.0 cm breadth × 0.5 cm thickness). The geometric area of each set of anodic meshes was 8.5 cm^2 and hence, the

two sets accounted for a total anodic area of 17 cm^2. The specific area (A/V_e) of each cathode (60 ppi RVC) was 40 cm^{-1} [28], yielding a total cathodic geometric area of 180 cm^2. Each of the anodic sets and RVC pieces was put in contact with a current collector with dimensions of 1.5 cm length × 3.0 cm breadth (Fig. 1a). For the anodes, Ti|IrO_2-Ta_2O_5 plates welded to screws made with the same material were employed, whereas stainless steel 3016 was used for the cathodes. The liquid inlet (diameter of 1.1 cm) was placed at the bottom of the cell. The solution was immediately dispersed to the channel through the manifold, which had five slots that directly connected to a receiving plastic net (Fig. 1a). The purpose of this net was to homogenize the fluid before it reached the first anode. When the solution came out from the second cathode, it was received by a plastic net, which was followed by the exit manifold made of five slots that dispersed the liquid toward the outlet (diameter of 1.1 cm).

The electrochemical reactor was connected to a closed reservoir by means of a hydraulic system made of polyvinyl chloride (PVC), and it was operated in recirculation mode (Fig. 2) to carry out the H_2O_2 accumulation. The tank contained 2 L of solution, which was recirculated using a magnetic pump model 4-MD-HC from Little Giant, with 0.1 horsepower (~75 W). It was adapted to a valve and flow meter model F-440 from Blue-White industries, with a maximum capacity of 1.0 L min^{-1} to control the flow rate. A BK Precision 1621A power source was employed to run the electrolyses at constant current and directly monitor the cell voltage. As mentioned above, an air pump was not needed because O_2 was collected from anodic OER.

2.2. Bulk electrolysis

The H_2O_2 accumulation trials were performed using 2 L of a 0.050 M Na_2SO_4 solution at pH 3.0 and room temperature (298 ± 2 K). The content of the electrogenerated oxidant

was quantified from the formation of the titanic-hydrogen peroxide yellowish complex [17], whose absorbance was measured employing a Perkin Elmer Lambda 35 spectrophotometer set at λ = 408 nm. The effect of the volumetric flow rate within the range 0.4-1.0 L min^{-1} and that of the constant applied current in the interval 59.5-178.5 mA (i.e., anodic current density in the range 3.5-10.5 mA cm^{-2}) on the time course of H_2O_2 concentration was studied. The electrolyte was deaerated before each electrolytic trial.

The current efficiency (ϕ) and the electrolytic energy consumption (EC) were the two figures of merit assessed during the accumulation of H_2O_2, being determined via Eq. (3) and (4):

$$\phi = \frac{nFC_{\mathrm{H_2O_2}}V}{1000M_{\mathrm{H_2O_2}}It} \times 100 \quad (3)$$

$$\mathrm{EC} = \frac{E_{\mathrm{cell}}It}{C_{\mathrm{H_2O_2}}V} \quad (4)$$

where n (=2) is the number of transferred electrons according to reaction (1), F is the Faraday constant (= 96,485 C per mol of electrons), $c_{\mathrm{H_2O_2}}$ is the hydrogen peroxide concentration (in mg L^{-1}), V is the solution volume (in L), $M_{\mathrm{H_2O_2}}$ is the molecular weight of H_2O_2 (34.01 g mol^{-1}), I is the applied current (in A), t is the electrolysis time (in s) and 100 is a conversion factor to determine the efficiency as a percentage. E_{cell} is the cell voltage (in V) resulting during the electrolysis. Note that, in this work, the EC values provided only take into account the electricity used to run the electrolysis, disregarding that needed to pump the solutions.

3. Results and discussion

Fig. 3a-c shows the influence of the flow rate on the H_2O_2 concentration profile, current efficiency and electrolytic energy consumption for the electrolysis of 2 L of a 0.050 M Na_2SO_4 solution at pH 3.0, maintaining a constant applied current of 59.5 mA for180 min. From the time course shown in Fig. 3a, a gradual increase of the oxidant concentration is evidenced at all flow rate values, which demonstrates the feasibility of two-electron ORR via reaction (1) in the reactor developed here without requiring air bubbling. Furthermore, the dependence of the reactor performance on the flow rate also confirms that reaction (1) is mass-transport controlled, i.e., it is a function of the arrival of the dissolved O_2 and the protons to the RVC cathode surface [15,17]. Not all the O_2 evolving at the anode via reaction (2) is completed dissolved [30], which is a drawback because O_2 in gas form is not adequate to be reduced. However, RVC is a suitable material, since its porous structure can act as a gas diffusor that breaks the gas bubbles and yields smaller microbubbles that can be finally dissolved to undergo the cathodic reduction [17,28].

A positive effect of the rising flow rate on the H_2O_2 accumulation was observed up to 0.8 L min^{-1}. Specifically, an almost 2.5-fold rise, from 6.1 to 14.3 mg L^{-1} at the end of the electrolysis, was achieved operating the system at 0.2 and 0.8 L min^{-1}, respectively. Worth noting, at 0.8 L min^{-1}, an abrupt increase of H_2O_2 concentration up to 6.7 mg L^{-1} can be seen during the first 20 min of electrolysis, clearly outperforming the trials made at lower or higher flow rates. This behavior can be plausibly related to the fast transport of the dissolved O_2 microbubbles to the cathode surface once generated at the anode, avoiding their coalescence and thus favoring their penetration through the RVC pores with the right dimensions. After that initial period, the H_2O_2 accumulation became slower due to its concomitant partial destruction.

Conversely, it seems that a greater flow rate of 1.0 L min^{-1} was detrimental from the point of view of the mass transport, attaining a lower H_2O_2 content of 10.4 mg L^{-1} at 180 min. This can be explained by at least of the following reasons: (i) the excessive transport of H^+ toward the RVC cathode surface, consequently stimulating the parasitic hydrogen evolution reaction (HER) via reaction (5) over the two-electron ORR; (ii) the enhanced transport of electrogenerated H_2O_2, either throughout the porous cathode favoring its reduction via reaction (6) or through the anode holes increasing its oxidation rate from the inverse of reaction (1); or (iii) the insufficient residence time of the dissolved O_2 within the cathode pores, limiting the extent of the ORR via reaction (1). Additionally, the greater hydrodynamic pressure could eventually favor the solution penetration within the RVC cathode, which would alter the area of the $O_{2(aq)}$-cathode interface, thereby promoting the cathodic H_2O_2 reduction reaction (6) [15,17].

$$2H^+ + 2e^- \rightarrow H_2 \qquad E° = 0 \text{ V vs SHE} \qquad (5)$$

$$H_2O_2 + 2H^+ + 2e^- \rightarrow 2H_2O \qquad E^0 = 1.801 \text{ V vs SHE} \qquad (6)$$

It is important to mention that the range of H_2O_2 concentrations determined in this new reactor with self-sustained H_2O_2 production are adequate for a future application to EF treatment of organic pollutants. For example, raw carbon-felt cathode produces about 7 mg H_2O_2 L^{-1} at moderate current densities in conventional EF reactors [29]. Within this context, it also interesting to note, in all the curves of Fig. 3a, the absence of a clear plateau at 180 min. This means that the H_2O_2 production rate is still greater than the consumption rate at that time, which is beneficial since it would allow to perform degradation experiments that can be prolonged for a long time without a lack of oxidant.

Fig. 3b illustrates the resulting current efficiency increase at higher flow rate within the interval of 0.2-0.8 L min^{-1}. The highest efficiency (100%) was obtained at 0.8 L min^{-1}

after 20 min, in correspondence with the unexpectedly large H_2O_2 concentration. Afterwards, it decreased exponentially during the electrolysis, reaching 25% at the end of the trial. The loss of current efficiency may be attributed to the aforementioned H_2O_2 consumption reactions, whose rate is enhanced as the accumulation becomes higher, although the partial H_2O_2 disproportionation of H_2O_2 in the bulk cannot be discarded either. At the other flow rates, the efficiency was quite constant in each single trial, which is a positive feature since it allows predicting very well the performance of the reactor. On the other hand, the EC curves agreed perfectly with the efficiency tendencies, revealing a lower consumption as the flow rate increased from 0.2 to 0.8 L min^{-1} (Fig. 3c). At 180 min, the lowest EC value attained at 0.8 L min^{-1} was 0.021 kWh (g H_2O_2)$^{-1}$.

A second set of electrolytic trials was performed to evaluate the influence of applied current on the electrosynthesis of H_2O_2, Fig. 4. These tests were carried out at a flow rate of 0.8 L min^{-1} and at constant applied current values of 59.5, 119 and 178.5 mA. These values were selected among others, as a better performance regarding the accumulation of H_2O_2 could not be obtained outside this range. Fig. 4a shows a lower H_2O_2 accumulation as applied current became higher. This means that, even though the OER is favored as the electrons are withdrawn more quickly from the anode (reaction (2)), thus saturating the solution with dissolved O_2, the cathodic potential is concomitantly shifted to more negative values. This favors the four-electron ORR to yield H_2O instead of H_2O_2 (i.e., inverse of reaction (2)), as well as the parasitic reactions (5) and (6) [15,17]. As a result, 13.2 and 10.6 mg H_2O_2 L^{-1} were obtained after 180 min at 119 and 178.5 mA, respectively.

Similarly, the current efficiencies became lower at any given time as the applied currents were increased (Fig. 4b), ending in 11.2% and 6.0% at 119 and 178.5 mA, respectively. Fig. 4c shows that the electrolytic energy consumption increased with the applied current,

which is directly related to the rise in cell potential, attaining values of 3.2, 4.5 and 6.0 V at 59.5, 119 and 178.5 mA, respectively. The greatest EC value was attained at 178.5 mA, being 0.157 kWh (g H_2O_2)$^{-1}$ after 180 min. The best performance of the reactor was achieved at 59.5 mA, reaching 14.3 mg L^{-1} H_2O_2 after 3 h, with current efficiency and electrolytic energy consumption of 24.2% and 0.021 kWh (g H_2O_2)$^{-1}$, respectively.

Conclusions

The electrosynthesis of H_2O_2 sustained by O_2 produced on site from water discharge is feasible in a well-engineered flow-through reactor equipped with Ti|IrO_2-Ta_2O_5 and RVC as the anode and cathode material, respectively. The experimental characterization of the reaction environment in terms of volumetric flow rate and applied current has been systematically studied by means of bulk electrolyses operating in recirculation mode. The best performance of the reactor has been achieved at 0.8 L min^{-1} and 59.5 mA, reaching 14.3 mg L^{-1} H_2O_2 after 3 h of electrolysis, with final current efficiency and electrolytic energy consumption of 24.2% and 0.021 kWh (g H_2O_2)$^{-1}$, respectively. The moderate concentration of H_2O_2 obtained in this first approach is estimated to be sufficient to produce hydroxyl radicals from Fenton's and peroxone reactions, with direct application in water treatment.

Acknowledgements

The authors are grateful for the financial support from project No. CIIC 113/2020 (University of Guanajuato, Mexico) and CTQ2016-78616R (AEI/FEDER, EU). O.M. Cornejo thanks CONACYT for the scholarship No. 708693 granted.

References

[1] R.J. Lewis, G.J. Hutchings, Recent advances in the direct synthesis of H_2O_2, ChemCatChem 11 (2019) 298-308.

[2] W. Zhou, X. Meng, J. Gao, A.N. Alshawabkeh, Hydrogen peroxide generation from O_2 electroreduction for environmental remediation: A state-of-the-art review, Chemosphere 225 (2019) 588-607.

[3] T. Nishimi, T. Kamachi, K. Kato, T. Kato, K. Yoshizawa, Mechanistic study on the production of hydrogen peroxide in the anthraquinone process, Eur. J. Org. Chem. 22 (2011) 4113-4120.

[4] F. Gozzi, I. Sirés, A. Thiam, S.C. de Oliveira, A.M. Junior, E. Brillas, Treatment of single and mixed pesticide formulations by solar photoelectro-Fenton using a flow plant, Chem. Eng. J. 310 (2017) 503-513.

[5] H. Lin, N. Oturan, J. Wu, H. Zhang, M.A. Oturan, Cold incineration of sucralose in aqueous solution by electro-Fenton process, Sep. Purif. Technol. 173 (2017) 218-225.

[6] Y. Wang, G. Yu, S. Deng, J. Huang, B. Wang, The electro-peroxone process for the abatement of emerging contaminants: Mechanisms, recent advances, and prospects, Chemosphere 208 (2018) 640-654.

[7] S. Lanzalaco, I. Sirés, M.A. Sabatino, C. Dispenza, O. Scialdone, A. Galia, Synthesis of polymer nanogels by electro-Fenton process: investigation of the effect of main operation parameters, Electrochim. Acta 246 (2017) 812-822.

[8] R. Ciriminna, L. Albanese, F. Meneguzzo, M. Pagliaro, Hydrogen peroxide: A key chemical for today's sustainable development, ChemSusChem 9 (2016) 3374-3381.

[9] H.-J. Riedl, G. Pfleiderer, Production of hydrogen peroxide, U.S. Patent 2,215,883, 24 September 1940.

[10] J.M. Barazesh, T. Hennebel, J.T. Jasper, D.L. Sedlak, Modular advanced oxidation process enabled by cathodic hydrogen peroxide production, Environ. Sci. Technol. 49 (2015) 7391-7399.

[11] I. Salmerón, K.V. Plakas, I. Sirés, I. Oller, M.I. Maldonado, A.J. Karabelas, S. Malato, Optimization of electrocatalytic H_2O_2 production at pilot plant scale for solar-assisted water treatment, Appl. Catal. B: Environ. 242 (2019) 327-336.

[12] O. González-Pérez, J.M. Bisang, Electrochemical synthesis of hydrogen peroxide with a three-dimensional rotating cylinder electrode, J. Chem. Technol. Biotechnol. 89 (2014) 528-535.

[13] Y. Liu, X. Quan, X. Fan, H. Wang, S. Chen, High-yield electrosynthesis of hydrogen peroxide from oxygen reduction by hierarchically porous carbon, Angew. Chem. 127 (2015) 6941-6945.

[14] X. Yu, M. Zhou, G. Ren, L. Ma, A novel dual gas diffusion electrodes system for efficient hydrogen peroxide generation used in electro-Fenton, Chem. Eng. J. 263 (2015) 92-100.

[15] G. Coria, T. Pérez, I. Sirés, J.L. Nava, Mass transport studies during dissolved oxygen reduction to hydrogen peroxide in a filter-press electrolyzer using graphite felt, reticulated vitreous carbon and boron-doped diamond as cathodes, J. Electroanal. Chem. 757 (2015) 225-229.

[16] Z. Pan, K. Wang, Y. Wang, P. Tsiakaras, S. Song, *In-situ* electrosynthesis of hydrogen peroxide and wastewater treatment application: A novel strategy for graphite felt activation, Appl. Catal. B: Environ. 237 (2018) 392-400.

[17] T. Pérez, G. Coria, I. Sirés, J.L. Nava, A.R. Uribe, Electrosynthesis of hydrogen peroxide in a filter-press flow cell using graphite felt as air-diffusion cathode, J. Electroanal. Chem. 812 (2018) 54-58.

[18] A. El-Ghenymy, N. Oturan, M.A. Oturan, J.A. Garrido, P.L. Cabot, F. Centellas, R.M. Rodríguez, E. Brillas, Comparative electro-Fenton and UVA photoelectro-Fenton degradation of the antibiotic sulfanilamide using a stirred BDD/air-diffusion tank reactor, Chem. Eng. J. 234 (2013) 115-123.

[19] G. Coria, T. Pérez, I. Sirés, E. Brillas, J.L. Nava, Abatement of the antibiotic levofloxacin in a solar photoelectro-Fenton flow plant: Modeling the dissolved organic carbon concentration-time relationship, Chemosphere 198 (2018) 174-181.

[20] B. Garza-Campos, D. Morales-Acosta, A. Hernández-Ramírez, J.L. Guzmán-Mar, L. Hinojosa-Reyes, J. Manríquez, E.J. Ruiz-Ruiz, Air diffusion electrodes based on synthetized mesoporous carbon for application in amoxicillin degradation by electro-Fenton and solar photo electro-Fenton, Electrochim. Acta 269 (2018) 232-240.

[21] Z. Ye, D.R.V. Guelfi, G. Álvarez, F. Alcaide, E. Brillas, I. Sirés, Enhanced electrocatalytic production of H_2O_2 at Co-based air-diffusion cathodes for the photoelectro-Fenton treatment of bronopol, Appl. Catal. B: Environ. 247 (2019) 191-199.

[22] Q. Zhu, Z. Pan, S. Hu, J.-H. Kim, Cathodic hydrogen peroxide electrosynthesis using anthraquinone modified carbon nitride on gas diffusion electrode, ACS Appl. Energy Mater. 2 (2019) 7972-7979.

[23] J.F. Pérez, J. Llanos, C. Sáez, C. López, P. Cañizares, M.A. Rodrigo, The jet aerator as oxygen supplier for the electrochemical generation of H_2O_2, Electrochim. Acta 246 (2017) 466-474.

[24] M. Panizza, G. Cerisola, Direct and mediated anodic oxidation of organic pollutants, Chem .Rev. 109 (2009) 6541-6569.

[25] P. Drogui, S. Elmaleh, M. Rumeau, C. Bernard, A. Rambaud, Oxidising and disinfecting by hydrogen peroxide produced in a two-electrode cell, Water Res. 35 (2001) 3235-3241.

[26] W. Zhou, L. Rajic, Y. Zhao, J. Gao, Y. Qin, A.N. Alshawabkeh, Rates of H_2O_2 electrogeneration by reduction of anodic O_2 at RVC foam cathodes in batch and flow-through cells, Electrochim. Acta 277 (2018) 185-196.

[27] Z.G. Aguilar, O. Coreño, M. Salazar, I. Sirés, E. Brillas, J.L. Nava, Ti|Ir-Sn-Sb oxide anode: Service life and role of the acid sites content during water oxidation to hydroxyl radicals, J. Electroanal. Chem. 820 (2018) 82-88.

[28] F.C. Walsh, L.F. Arenas, C. Ponce de León, G. Reade, I. White, B.G. Mellor, The continued development of reticulated vitreous carbon as a versatile electrode material: Structure, properties and applications, Electrochim. Acta 215 (2016) 566-591.

[29] I. Sirés, J.A. Garrido, R.M. Rodríguez, E. Brillas, N. Oturan, M.A. Oturan, Catalytic behavior of the Fe^{3+}/Fe^{2+} system in the electro-Fenton degradation of the antimicrobial chlorophene, Appl. Catal. B: Environ. 72 (2007) 382-394.

[30] K. Klunder, F.A. Hekman, K.L. Brown, G.F. Peaslee, A study of dissolved gas dynamics in mixed stream electrolyzed water, Electrochem. 80(8) (2012) 574-577.

Figure captions

Fig. 1. (a) Exploded view of the flow-through reactor and (b) liquid flow channel.

Fig. 2. Electrical and flow circuit employed for the bulk electrolyses.

Fig. 3. Influence of volumetric flow rate on the (a) H_2O_2 accumulation, (b) current efficiency (c) and electrolytic energy consumption. Electrolyte: 0.050 M Na_2SO_4 at pH 3.0 and 298 ± 2 K. The applied current was 59.5 mA. The geometric area of the anode and cathode was 17 cm^2 and 180 cm^2, respectively.

Fig. 4. Influence of applied current on the (a) H_2O_2 accumulation, (b) current efficiency (c) and electrolytic energy consumption. Same conditions described in Fig. 3, at a volumetric flow rate of 0.8 L min^{-1}.

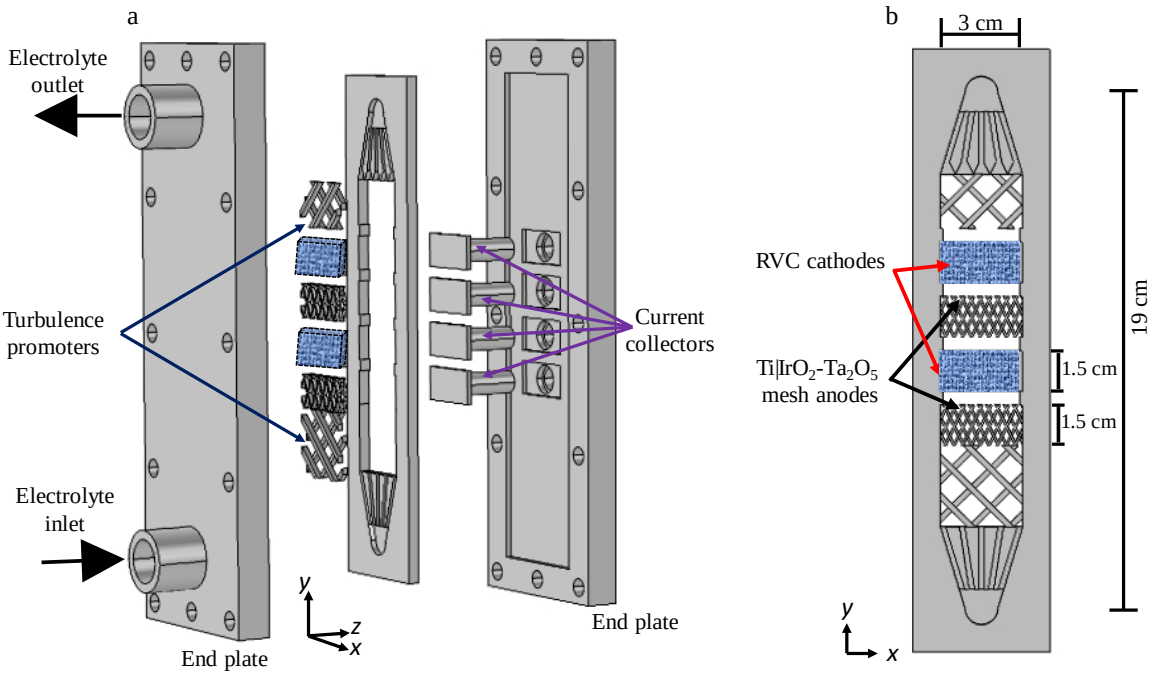
a
Electrolyte outlet
Turbulence promoters
Electrolyte inlet
End plate
Current collectors
End plate
y
z
x
b
3 cm
RVC cathodes
Ti|IrO2-Ta2O5 mesh anodes
1.5 cm
1.5 cm
19 cm
y
x

Figure 1

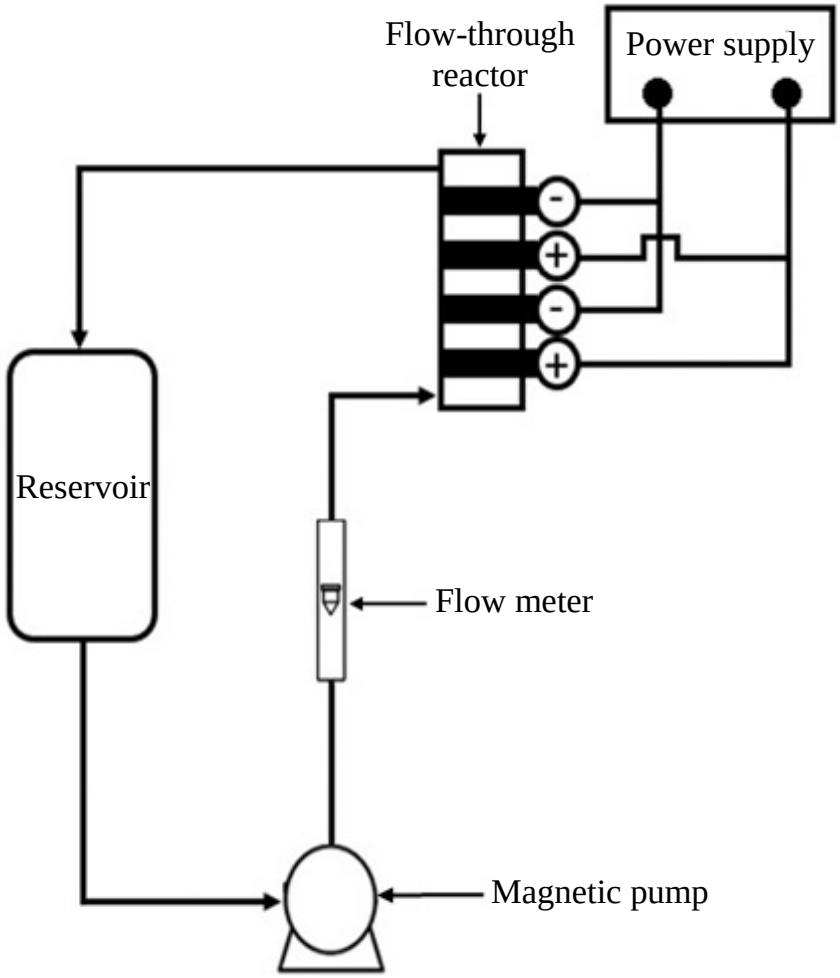
Flow-through
reactor
Power supply
Reservoir
Flow meter
Magnetic pump

Figure 2

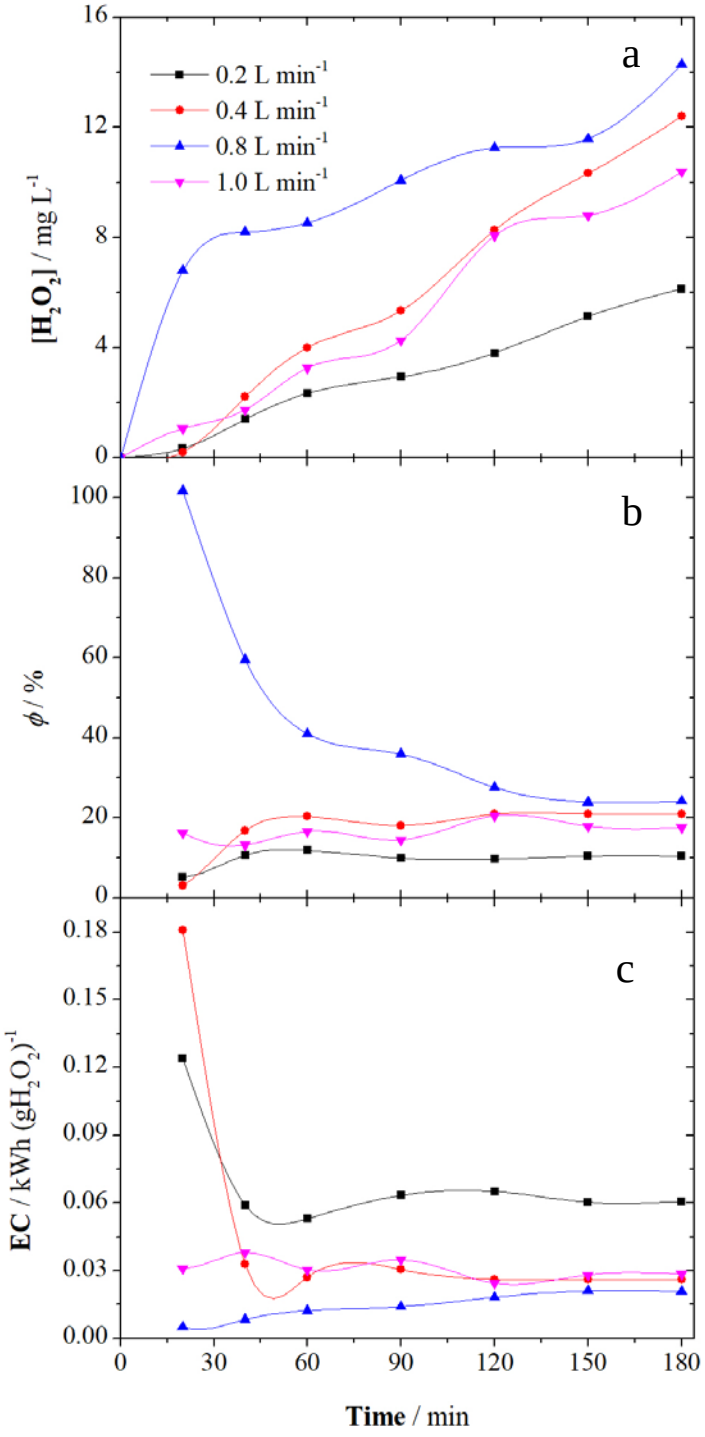
a
b
c
0.2 L min-1
0.4 L min-1
0.8 L min-1
1.0 L min-1
[H2O2] / mg L-1
ϕ / %
EC / kWh (gH2O2)-1
Time / min
0
4
8
12
16
20
40
60
80
100
0.00
0.03
0.06
0.09
0.12
0.15
0.18
0
30
60
90
120
150
180

Figure 3

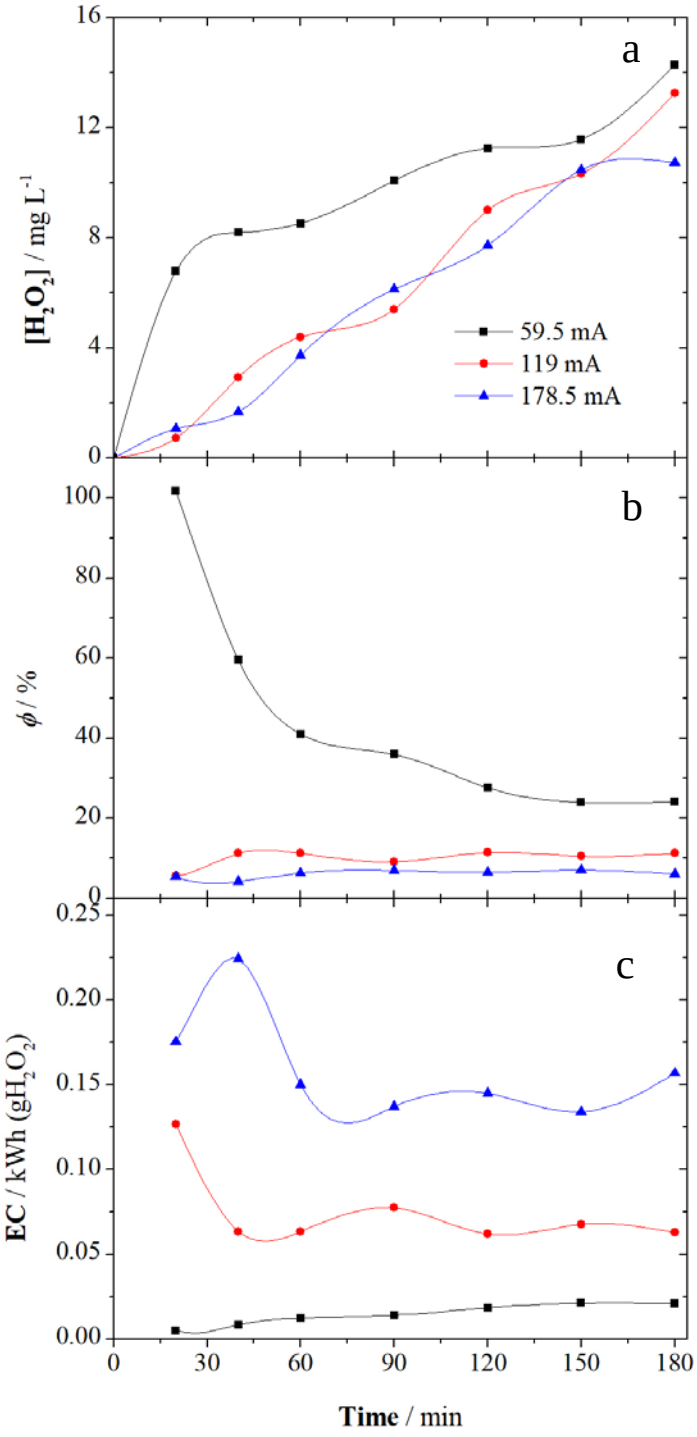
a
b
c
59.5 mA
119 mA
178.5 mA
[H2O2] / mg L-1
ϕ / %
EC / kWh (gH2O2)
Time / min
0
4
8
12
16
20
40
60
80
100
0.00
0.05
0.10
0.15
0.20
0.25
30
60
90
120
150
180

Figure 4

Table 1. Dimensions and characteristics of the reactor and the electrodes.

Channel length	19 cm
Channel breadth	3 cm
Channel thickness	0.5 cm
Electrode spacing	0.5 cm
Turbulence promoter, plastic mesh Type D	DC[a] and DL[b] = 1.1 cm
Volumetric area (RVC)	40 cm^{-1}
RVC porosity	0.965
RVC area in contact with the solution	180 cm^2
Ti|IrO_2-Ta_2O_5 anode area, in contact with the solution	17 cm^2

[a] Internal dimension of the short diagonal of the mesh

[b] Internal dimension of the long diagonal of the mesh